APPLIED ORGANOMETALLIC CHEMISTRY
Appl. Organometal. Chem. 2006; **20**: 648–655
Published online 7 August 2006 in Wiley InterScience
(www.interscience.wiley.com) DOI:10.1002/aoc.1135

UV laser deposition of nanostructured Si/C/O/N/H from disilazane precursors and evolution to silicon oxycarbonitride

Josef Pola[1]*, Anna Galíková[1], Zdeněk Bastl[2], Jan Šubrt[3], Karel Vacek[1], Jiří Brus[4] and Akihiko Ouchi[5]*

[1]Laboratory of Laser Chemistry, Institute of Chemical Process Fundamentals, Academy of Sciences of the Czech Republic, 16502 Prague, Czech Republic
[2]J. Heyrovský Institute of Physical Chemistry, Academy of Sciences of the Czech Republic, 18223 Prague 8, Czech Republic
[3]Institute of Inorganic Chemistry, Academy of Sciences of the Czech Republic, 25068 Řež, Czech Republic
[4]Institute of Macromolecular Chemistry, Academy of Sciences of the Czech Republic, 16206 Prague 6, Czech Republic
[5]National Institute of Advanced Industrial Science and Technology, AIST, Tsukuba, Ibaraki 305-8565, Japan

Received 28 March 2006; Revised 24 April 2006; Accepted 8 June 2006

Megawatt ArF laser photolysis of gaseous methyldisilazanes $[(CH_3)_nH_{3-n}Si]_2NH$ ($n = 2, 3$) in excess of Ar yields hydrocarbons (major volatile products), methylsilanes (minor volatile products) and allows chemical vapour deposition of solid amorphous Si/C/O/N/H powder containing Si–X (X=C, H, O, N) bonds. The incorporation of O is due to a high reactivity of the primarily formed products towards air moisture. The resulting solid materials possess nanometer-sized texture and high specific area, contain Si-centered radicals and anneal under argon to silicon oxycarbonitride, whose structure is described as a network of O- and N-interconnected Si and C atoms. Copyright © 2006 John Wiley & Sons, Ltd.

KEYWORDS: laser-induced photolysis; methyldisilazanes; chemical vapour deposition; oxycarbonitride

INTRODUCTION

Silicon oxycarbide and silicon nitride materials of high temperature and chemical stability attract continuing attention. Their synthesis was achieved through thermolytic conversion of oxygen- and nitrogen-containing organosilicon precursors, mostly oligomeric and polymeric crosslinked siloxanes[1–3] or polysilazanes.[4–7] Another and simpler approach towards Si/C/O and SiC/N phases is based on interaction of infrared or ultraviolet laser radiation with gaseous or aerosol forms of organosilicon monomers. Ultrafine preceramic Si/C/N[8,9] or Si/C/O[10,11] powders were obtained by ultrasonic injection of aerosol particles of hexamethyldisilazane and hexamethyldisiloxane into a high-power CO_2 laser beam through laser-induced thermolysis of the organosilicon precursors.

*Correspondence to: Josef Pola or Akihiko Ouchi, Laboratory of Laser Chemistry, Institute of Chemical Process Fundamentals, Academy of Sciences of the Czech Republic, 16502 Prague, Czech Republic.
E-mail: pola@icpf.cas.cz
Contract/grant sponsor: Ministry of Education, Youth and Sports of the Czech Republic; Contract/grant number: ME 684.

Another interesting family of preceramic materials[12] are organosilicon oxycarbide nitrides, which incorporate siloxane and silazane bonds and can serve as precursors to silicon oxynitride. The silicon oxynitride, $SiO_xN_yH_z$, finds many applications in electronics and ceramics and its synthesis was mostly achieved by plasma-enhanced chemical vapour deposition (CVD) technique applied to hazardous chemicals (chlorohydridosilanes or silane).[13–16] There are only two reports on silicon oxynitride (more specifically silicon oxycarbonitride, $SiC_tO_xN_yH_z$) synthesis from safe methylsilazanes: a conventional CVD in the presence of N_2O[17] and the plasma-induced CVD in the presence of oxygen and ammonia.[18]

We have previously described IR laser-induced pyrolytic approach to various Si/C/O and Si/O phases from gaseous organosilicon precursors.[19–21] We have also shown that the Si/C/O and Si/O nano-structured solid phases can be prepared by interaction of gaseous organosilicon precursors with strong UV laser field[22–24] at room-temperature of the whole volume of the irradiated gas phase.

Here we report on MW UV laser photolysis of gaseous hexamethyldisilazane (HMDSZ) and 1,1,3,3-tetramethyldisilazane (TMDSZ) {$[(CH_3)_nH_{3-n}Si]_2NH$, $n = 2, 3$} and show that this procedure affords CVD of an ultrafine solid that undergoes partial hydrolysis upon exposure to air and can be subsequently annealed to silicon oxycarbonitride.

EXPERIMENTAL

The ArF laser photolytic experiments were carried out on gaseous samples of HMDSZ (12 Torr, 10^{-4} mol) or TMDSZ (28 Torr, 2.3×10^{-4} mol) in argon (total pressure 760 Torr) using an LPX 210i laser (ArF radiation) operating at 193 nm with a pulse energy of 200 mJ and a repetition frequency of 10 Hz. The gaseous samples were irradiated with a focused laser beam (pulse width 23 ns, fluence 2.5 J cm^{-2}, the incident pulse effective on 8×10^{-2} cm^2) in a Pyrex reactor (140 ml in volume). These irradiation conditions correspond to the total output of over 10 MW. The reactor was equipped with a sleeve with a rubber septum and a PTFE valve connecting it to a standard vacuum manifold and consisted of two orthogonally positioned Pyrex tubes, one fitted with two quartz plates and the other furnished with two KBr windows. The excess of Ar prevents leakage of traces of air moisture into the reactor and phydrolysis of disilazanes. The reactor surface was pretreated with HMDSZ and TMDSZ.

The progress of the photolysis was monitored directly in the reactor by FTIR spectrometry (a Shimadzu FTIR 4000 spectrometer) using respective absorption bands of HMDSZ and TMDSZ at 687 and 772 cm^{-1}.

The analysis of the volatile products was performed by FTIR spectroscopy (ethyne at 730 cm^{-1} and methane at 3016 and 1305 cm^{-1}), by GC-MS method (a Shimadzu QP 5050 mass spectrometer (60 m capillary column Neutrabond-1, programmed temperature 30–200 °C) and by gas chromatography [a Shimadzu 14A chromatograph equipped with a 2 m long Porapak column, programmed (30–150 °C) temperature and connected with a Shimadzu CR 5A data processor]. Sampling was made by a gas-tight syringe (Dynatech Precision Sampling).

The reactor accommodated KBr substrates which, covered with the deposited materials, were measured for their FTIR spectra directly in the evacuated reactor. The obtained solid deposits were removed from the reactor and transferred (not avoiding a short contact with air) for measurements by electron paramagnetic (EPR) and X-ray photoelectron (XP) and nuclear magnetic resonance (NMR) spectroscopy and by electron microscopy in closed ampoules.

The FTIR spectra of the solid films deposited on KBr were acquired on a Shimadzu FTIR 4000 spectrometer.

The EPR spectra of the deposited ultrafine powders obtained from TMDSZ (2.6 mg) and HMDSZ (1.7 mg) and of the solids obtained from them by annealing under argon atmosphere to 700 °C (0.62 and 0.63 mg, respectively) were measured at room temperature in air by a continuous-wave EPR spectrometer working in X band (9.3 GHz and 1 mW) with 100 kHz magnetic field modulation (0.115 mT). The spectrometer was equipped with a digital frequency counter and an NMR magnetometer used for g-factor calculation. Quantitative estimation of spin concentration is based on TEMPOL and Mn^{2+} (internal standard). The solid from TMDSZ annealed to 700 °C was placed in a quartz EPR tube and irradiated with HBO 200 W mercury lamp (full spectrum radiation and the radiation filtered with the water solution of $CoSO_4$ (240 g/L) and with the ArF laser (repetition frequency 10 Hz, energy of 65 mJ per pulse). The samples were irradiated and measured at room temperature and at temperature of liquid nitrogen.

The XPS measurements were conducted using ESCA 310 (Gammadata Scienta) spectrometer and AlKα (1487 eV) radiation. The high-resolution spectra of Si (2s), Si (2p), C (1s), O(1s) and N (1s) were measured. Calculation of the concentration of elements was accomplished by correcting the photoelectron peak intensities for their cross-sections.

1D ^{13}C CP/MAS and ^{29}Si MAS NMR spectra were measured using a Bruker Advance 500 WB/US spectrometer using rotation frequency 12 kHz, intensity of $B_1(^1H)$ field for cross-polarization 62.5 kHz and recycle delay 3 s. Single-pulse experiments were carried out with a 45°-pulse length (2 μs) and 60 s repetition delay. $B_1(^1H)$ field intensity of TPPM (two-pulse phase-modulated) decoupling corresponds to $\omega_1/2\pi =$ 89.3 kHz. The number of scans was 1200. ^{29}Si and ^{13}C scales were calibrated by external standard M_8Q_8 (−109.8 ppm; the highest field signal) and glycine (176.03 ppm; carbonyl signal), respectively. The temperature of bearing inlet air was set to 23 °C and the temperature of the sample was higher by ca. 14 °C due to the frictional heating of the rotor.

The morphology of the solid materials was characterized by scanning electron microscopy (SEM), transmission electron microscopy (TEM) and by Brauner, Emmet and Teller (BET) surfaces. SEM photographs were obtained using a Philips XL30 CP scanning electron microscope and TEM photomicrographs were obtained using a Philips 201 transmission electron microscope. BET surfaces of the powders were measured using a Micromeritics Flowsorb 2300 instrument.

Thermal analysis of the solid deposits (sample weight 1.8–3 mg) was carried out by heating the samples to 700 °C at a rate of 4 °C min^{-1}, using a Cahn D-200 recording microbalances in a stream of argon. The composition of the outgoing gases was analysed by an automatic sampling gas chromatograph Hewlett-Packard GC5890 equipped with FID detector and Porapak P packed column (i.d. 2 mm, 2 m long). The sample residue remaining on the balance pan was analysed in a KBr tablet by FTIR spectroscopy and electron microscopy.

HMDSZ (purity 99.99%) and TMDSZ (purity ca. 95%) (both Aldrich) were commercial samples that were distilled prior to use.

DOI: 10.1002/aoc

RESULTS AND DISCUSSION

Laser photolysis

The gaseous disilazanes $[(CH_3)_nH_{3-n}Si]_2NH$ ($n = 2$, 3) can be photolysed by the ArF laser radiation, although their absorptivity at 193 nm is only 2.5×10^{-2} Torr^{-1} cm^{-1}. Each photolysis results in the formation of many volatile products. Hydrocarbons (ethane, ethyne), methylsilanes $(CH_3)_nSiH_{4-n}$ ($n = 2$–4), organosilicon compounds with two and three Si atoms containing NH and/or O unit, silazanes with CH_3–N group and also hydrogen cyanide and benzene were observed (Fig. 1). Concomitantly with the formation of the volatile compounds, a white fog was produced within all the reactor volume, which descended slowly on the reactor bottom to yield a white ultra-fine powder.

The energy delivered by the photons at 193 nm corresponds to ca. 620 kJ mol^{-1}, which is much in excess of the energy needed for the cleavage of the weaker Si–C (~370 kJ mol^{-1}), Si–H (~380 kJ mol^{-1}) and C–H (~410 kJ mol^{-1}) bonds, of the strongest Si–N (~420 kJ mol^{-1}) bond, and also for inducing three-centre elimination of silylenes and carbenes (~250–300 kJ mol^{-1}).[25,26]

The observed formation of hydrocarbons indicates cleavage of the Si–C bonds and that of methylsilanes confirms cleavage of the Si–N bond. The main Si–O bond-containing products (tetramethyldisiloxane and hexamethyldisiloxane, shown as respective peaks 11 and 14 in Fig. 1) were determined by gas chromatography to represent 5–10 mol% of the introduced disilazane precursor and their presence can be accounted for by a hardly avoidable low-extent hydrolysis on (pretreated) glass surface, or more likely by reactions of hot photolytic species with glass reactor surface. The C_2H_2, HCN and benzene are high-temperature products and reveal the occurrence of high degradation steps within the focused laser pulse, where energy density reaches more than 1 MW.

The observed distribution of the volatile products differs remarkably from the low-fluence ArF laser photolysis of hexamethyldisilazane when the major products are methane and trimethylsilane which are formed via [H]-abstraction by $(CH_3)_3Si^{\bullet}$ and $CH_3^{\bullet}$ radicals from H(C) and H(N) bonds and via 1,1-elimination of trimethylsilane.[27] These low-energy paths undoubtedly take place in the MW laser photolysis as primary steps.

Properties of powders

The powders obtained from both photolyses amounted to ca. 30–40 mg quantities when collected from six runs with TMDSZ (total 186 mg) and 10 runs with HMDSZ (total 180 mg), each photolytic run lasting 4 min. They are insoluble in organic solvents and difficult to handle due to their keeping an electrostatic charge.

Electron microscopy and surface properties

SEM analysis confirms that both powders have similar coral-like morphology (Fig. 2).

TEM analysis shows that the aggregates consist in chain-like ca. 30 nm-sized or greater agglomerates; typical TEM image is given in Fig. 3. Properties of both powders are illustrated in Table 1: the powders possess very similar stoichiometry and have very similar content of O. The

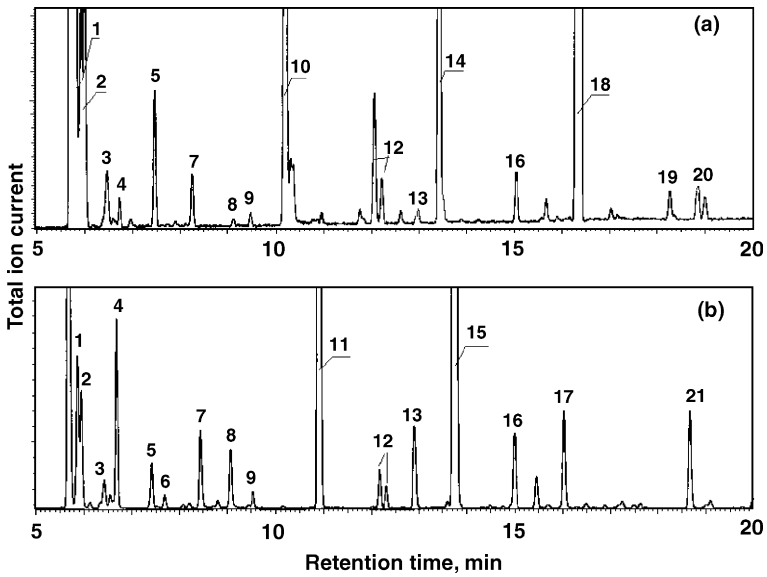

Figure 1. GC/MS trace of mixtures of volatile products formed in laser photolysis of hexamethyldisilazane (a) and 1,1,3,3-tetramethyldisilazane (b). Product designation: **1**, C_2H_2; **2**, C_2H_6; **3**, HCN; **4**, $(CH_3)_2SiH_2$; **5**, $(CH_3)_3SiH$; **6**, C_4H_2; **7**, $(CH_3)_4Si$; **8**, $(CH_3)_2SiHXH$; **9**, $(CH_3)_2(C_2H_5)SiH$; **10**, $(CH_3)_3SiXH$; **11**, $(CH_3)_2HSiOSi(CH_3)_2H$; **12**, $(CH_3)_4H_2Si_2X$; **13**, C_6H_6; **14**, $(CH_3)_3SiOSi(CH_3)_3$; **15**, 1,1,3,3-tetramethyldisilazane; **16**, $(CH_3)_3SiXNHSi(CH_3)_3$; **17**, $(CH_3)_2HSiXSi(CH_3)_2XSi(CH_3)_2H$; **18**, hexamethyldisilazane; **19**, $(CH_3)_3SiXSi(CH_3)_2XSi(CH_3)_3$; **20**, $[(CH_3)_3Si)_2NCH_3$; **21**, $[(CH_3)_2HSi]_3N$ (X=O, NH).

DOI: 10.1002/aoc

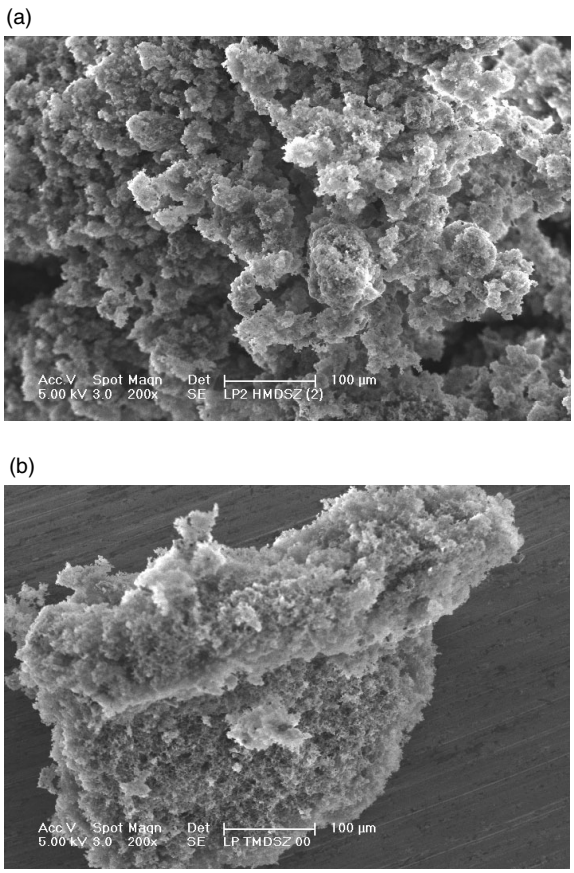

Figure 2. SEM images of the powders from HMDSZ (a) and TMDSZ (b). The bar equals 100 µm.

comparison of the EDX- and XPS-derived stoichiometry reveals that the content of O is greater in the topmost layers. These features indicate similar reactivity of both powders towards air moisture and show that a fraction of N is greater in deeper layers. Both powders have practically the same average pore diameter (124 and 127 Å), but that from HMDSZ has larger surface area. We note that the value of the average pore diameter in these powders is by two orders of magnitude lower than that in polyoxocarbosiloxane powders obtained by laser photolysis of disiloxanes.[28]

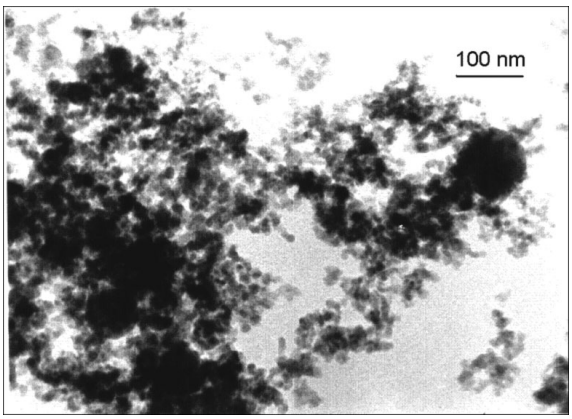

Figure 3. TEM image of the powder from TMDSZ.

EPR spectra

The EPR spectra of the powders [Fig. 4(a, b)] show a single asymmetric line with identical *g*-factor (2.0025) and without observable hyperfine structure. Evacuation of the samples to 5 Pa changes neither the shape nor the intensity of their EPR spectra and the annealing of the samples to 700 °C leads to a decrease of concentration of paramagnetic species (Table 2). The EPR spectra of the heated samples do not show hyperfine structure after irradiation by the Hg lamp or the ArF laser.

The greater line width (0.59 mT compared with 0.29 mT) correlates with a higher content of the Si–H bonds (as derived from the FTIR spectra, see later). This confirms the interaction of unpaired electron with hydrogen proton, which should have been resolved as a doublet, provided

Table 2. The linewidths and concentrations of paramagnetic species in deposited and annealed powders

Precursor	Temperature, °C	Linewidth, mT	Concentration, per g × 10^{-18}
TMDSZ	20	0.59	1.40
TMDSZ	700	0.59	1.21
HMDSZ	20	0.29	2.00
HMDSZ	700	0.29	0.68

Table 1. Properties of the deposited powders

	Disilazane precursor	
Property/analysis	$[(CH_3)_2HSi]_2NH$	$[(CH_3)_3Si]_2NH$
Precursor stoichiometry	$Si_1N_{0.5}C_2$	$Si_1N_{0.5}C_3$
EDX analysis	$Si_{1.00}C_{0.30}O_{1.23}N_{0.18}$	$Si_{1.00}C_{0.32}O_{1.22}N_{0.16}$
XPS analysis	$Si_{1.00}C_{0.15}O_{1.58}N_{0.03}$	$Si_{1.00}C_{0.12}O_{1.69}N_{0.02}$
BET surface area, $m^2\ g^{-1}$	156	104
Average pore diameter, Å	124	127
Concentration of unpaired spins per g	1.4×10^{18}	2.0×10^{18}

DOI: 10.1002/aoc

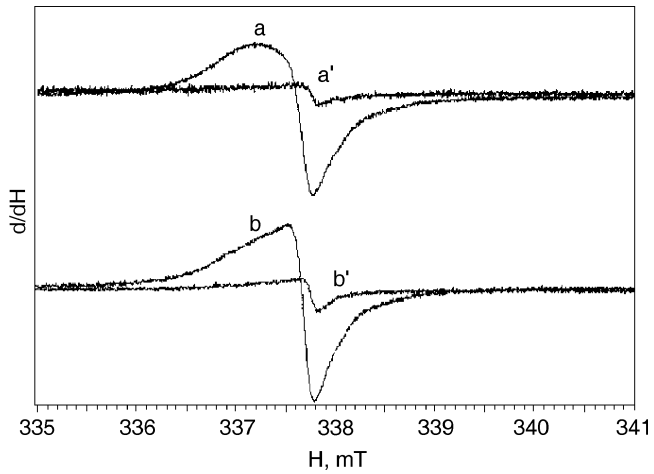

Figure 4. EPR spectrum of the powders obtained from TMDSZ (a) and HMDSZ (b) and the respective powders annealed to 700 °C (a′, b′).

that the EPR line was sufficiently intense and narrow. The *g*-factor 2.0025 is compatible with a $(Si_2O)Si^{\bullet}$ radical centre (*g*-factor = 2.0023). This assignment is in line with the well-known high thermal stability of this type of radical centre.[29,30] We note that the incorporation of nitrogen into amorphous silicon oxide matrix leads to the occurrence of paramagnetic centers accountable for by hyperfine spin interaction with N.[31] However, such interaction has not been detected even after long UV illumination of the samples, which is known[32] to enhance concentration of these species.

XP spectra

The Si (2p) spectra of the topmost (ca. 4 nm) layers in the deposited powders reveal the silicon at 101.6 eV (ca. 15%) and 103.3 eV (ca. 75%), which are respectively assigned[33,34] to a Si–C, Si–N, and/or Si–C–H structure and to a SiO_xN_y structure, respectively. The N (1s) signal is composed from a major (>90%) component at 397.8 eV and a minor (<10%) component at 401.5 eV; the former is tentatively assigned[35,36] to a nitrogen atom bonded to silicon. The C (1s) signal for both samples at 284.8 eV is compatible with carbon bonded to C, H and Si atoms.

FTIR spectra

The FTIR spectra of both powders have a similar pattern (Fig. 5) and show contributions of C–H, C–N, CH_3–Si, Si–O and Si–N bonds (Table 3). The spectrum of the powder from TMDSZ reveals the presence of Si–H bonds in an $HSiX_m$ group (X = N or O). The broad bands at 950–1200 cm^{-1} are in principle assignable to three components, namely Si–N–Si, Si–O–Si and Si–O–C stretches, while the region at 770–850 cm^{-1} is characteristic for Si–C stretches in siloxanes and silazanes. The broad bands at 3000–3600 cm^{-1} belong to associated H–X bonds (X = N, O).

Solid-state NMR spectra

In carbon NMR spectra measured with and without cross-polarization (^{13}C CP/MAS and ^{13}C MAS NMR) only one signal with chemical shift around 0.0 ppm was detected. This single signal clearly indicates relatively limited structural variation of carbon atoms directly bonded to silicon. On the other hand, much more complex pattern of NMR spectra is provided by ^{29}Si MAS and CP/MAS NMR experiments (Fig. 6). Both types of ^{29}Si NMR spectra, which are almost identical, clearly reflect wide range of Si structure units. Owing to relatively low resolution of ^{29}Si NMR spectra, we could perform only rough signal assignment. However, according to the literature[40,41] and our previous experiences with silicon–oxycarbide glasses[42] we can unambiguously identify following basic structure units: C_3SiO, C_4Si, C_2SiO_2, $CSiO_3$ and SiO_4 resonating at ca. 10, 0, −20, −60 and −100 ppm, respectively. As measurement of ^{13}C CP/MAS and ^{29}Si

Table 3. FTIR spectra of deposits

Wavenumber, cm^{-1}	Relative absorbance[a] powder from $[(CH_3)_2HSi]_2NH$	Relative absorbance[a] powder from $[(CH_3)_3Si]_2NH$	Assignment[b]
3000–3600	c	c	ν(X–H), X=N,H
2960		0.26	ν(C–H)
2130		—	ν(Si–H)
1376	0.70	0.46	ν(C–N)
1258	1.00	1.00	$\delta(CH_3–Si)$
1121 d	d	1.00	ν(SiOC)
1055 ± 5 c	3.25	3.70	ν(Si–X), X=O, N
904	1.75	—	δ(Si–H)
840 ± 5	1.15	1.20	$\rho(CH_3–Si)$
804	0.38	0.43	ν(Si–C)

[a] Normalized to A[$\delta(CH_3–Si)$] at 1258 cm^{-1}.
[b] References 37–39.
[c] Broad band.

DOI: 10.1002/aoc

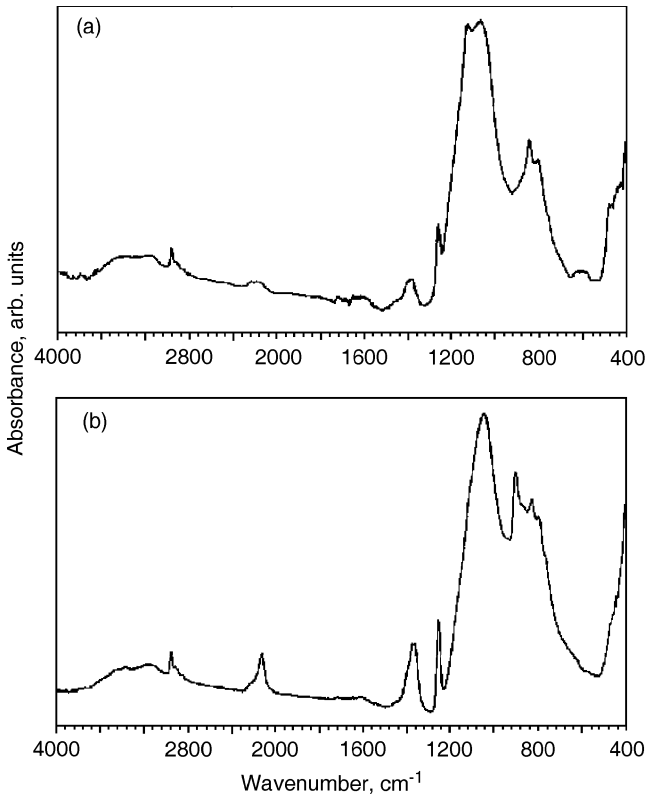

Figure 5. FTIR spectra of the deposit from HMDSZ (a) and TMDSZ (b).

CP/MAS NMR spectra employs polarization transfer from protons to carbon atoms, it is quite clear that all the detected silicon and carbon structure units must be close to hydrogen atoms. The maximum distance must not be larger than 0.4–0.5 nm.

Presence of silicon-oxynitride species $SiN_xO_{(4-x)}$ is plausible, since signals of these structure units usually appear in the range of chemical shift −20 to −70 ppm. However, they cannot be resolved from signals of $SiC_xO_{(4-x)}$ species. (We were not able to record ^{15}N MAS NMR spectrum with acceptable signal-to-noise ratio due to the low natural isotopic abundance of ^{15}N, relatively low content of nitrogen in the sample and expected very broad ^{15}N NMR signal, although the maximum experimental time was 24 h.)

Thermal behaviour

Thermograms of the powders (Figures 7, 8) show that the powders are quite stable, since they decrease their weight upon heating to 700 °C by at most 10% and do not change their whitish appearance.

The thermal degradation of the powder from HMDSZ [Fig. 8(a)] begins at *ca* 500 °C and gets its maximum at *ca* 650–700 °C, when the weight loss is due to the formation

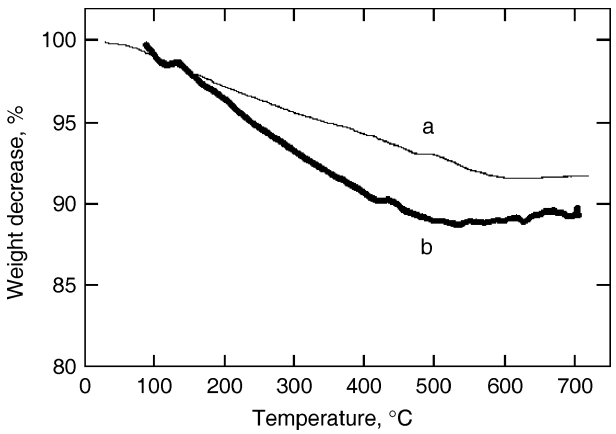

Figure 7. Thermogram of the deposits from HMDSZ (a) and TMDSZ (b).

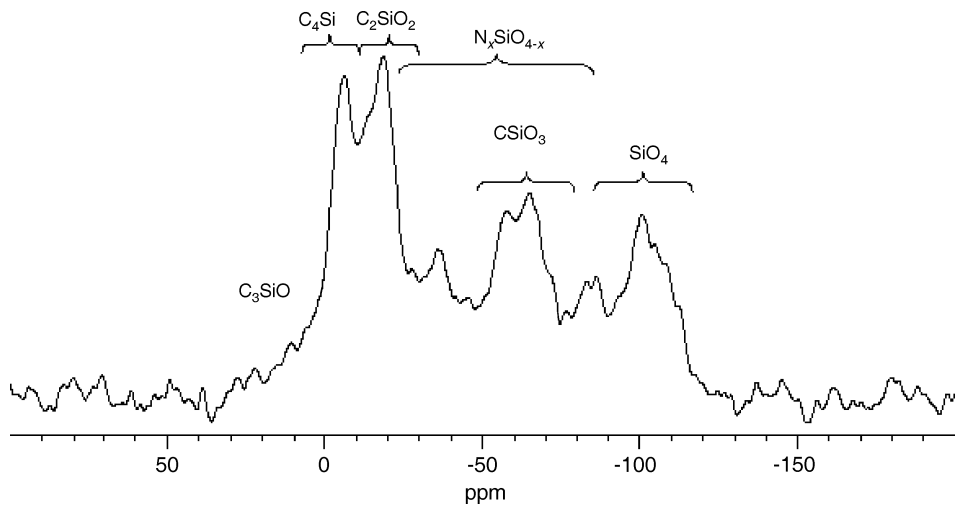

Figure 6. ^{29}Si MAS NMR spectrum with typical ranges of chemical shift of the detected structure units.

DOI: 10.1002/aoc

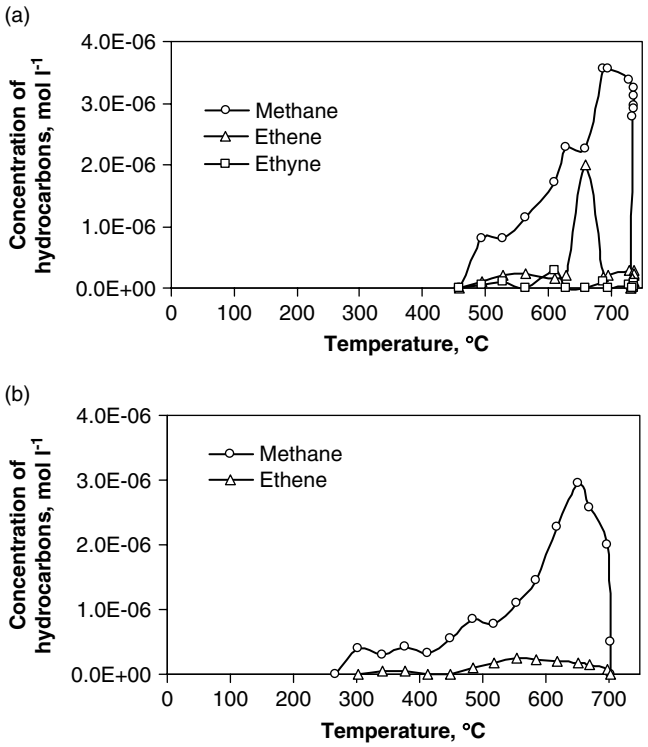

Figure 8. Gases evolved during TGA of deposit from HMDSZ (a) and TMDSZ (b).

of comparable amounts of methane and ethene. The thermal degradation of the powder from TMDSZ [Fig. 8(b)] begins at *ca* 300 °C and reaches its maximum at *ca* 650 °C, which is mostly caused by the formation of methane. The preferential formation of methane is in line with the presence of the Si–H bonds and is facilitated by combination of $CH_3^{\bullet}$ radicals and H atoms and/or by [H]-abstraction by $CH_3^{\bullet}$ radicals from the Si–H bonds. Ethene is formed through decomposition of $CH_3^{\bullet}$ radicals and combination of methylene ($CH_3^{\bullet} \rightarrow : CH_2 + H$, $2{:}CH_2 \rightarrow C_2H_4$).

The EDX-SEM analysis reveals that the relative content of Si, C, O and N elements in the deposited solids change slightly upon heating to 700 °C: the stoichiometry of the annealed solids ($Si_{1.00}C_{0.23-0.25}O_{1.23-1.30}N_{0.16}$) differs from that of the initially deposited solids (Table 1) by a lower content of carbon. This is in agreement with the observed evolution of the hydrocarbons. We note that the observed thermal behaviour of the deposits, resembling that of crosslinked polysiloxanes[1] and laser-fabricated polyoxocarbosilanes[24,28] suggests that the annealed materials can be best described as a highly crosslinked Si/C/N/O structure.

This view is corroborated by the FTIR spectra of the annealed powders, which are dominated by a broad band centered at ~1100 cm^{-1} and having a shoulder at 1200 cm^{-1}. The spectra also possess a week band at ~820 cm^{-1}, but do not show any ν(C–H) band. (The observed bands are shown in Fig. 9.)

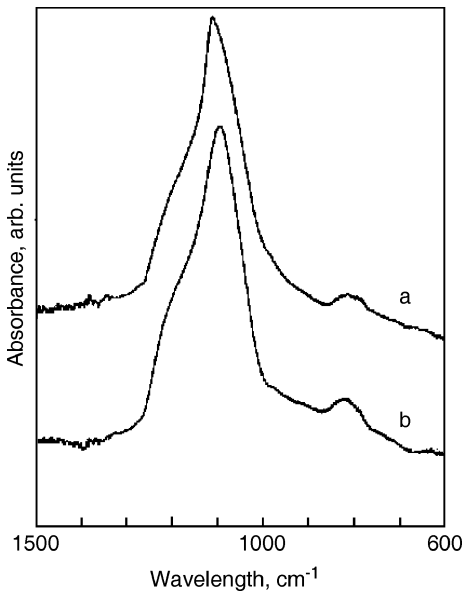

Figure 9. FTIR spectrum of the deposit from HMDSZ (a) and TMDSZ (b) annealed to 700 °C.

These features and the EDX-derived stoichiometry can be only reconciled by assigning the broad band to a blend of ν(SiOC), ν(SiOSi) and ν(SiNSi) vibration modes (whose maxima respectively appear at decreasing wavelength between 900 and 100 cm^{-1})[37] and by assigning the shoulder at 1200 cm^{-1} to a δ(NH) mode and the band at 820 cm^{-1} to a blend of ν(Si–C) and δ(Si–O) modes.[37] The lack of the $\delta(CH_3–Si)$ (at 1258 cm^{-1}) and of the ν(C–H) absorption bands (at 2960 cm^{-1}), which were observed in the spectra of the deposited samples (Table 2, Fig. 5), serves as evidence of a thermally induced reorganization of the initial structure into a Si/O/C/N/H network dominated by Si–O–X (X = C, Si) bridges.

CONCLUSIONS

The gas-phase MW ArF laser photolysis of methyldisilazanes $[(CH_3)_nH_{3-n}Si]_2NH$ ($n = 2$, 3) in excess Ar yields hydrocarbons (major volatile products), methylsilanes (minor volatile products) and allows chemical vapour deposition of amorphous ultrafine Si–C–H–O–N powders.

The identified products are compatible with a number of reaction steps occurring in a narrow region of the gaseous sample maintained at room temperature. The powders are very reactive towards air moisture and incorporate O. The modified powders have a high specific surface, possess nanometer-sized texture and contain unpaired electrons at the silicon atom in $(Si_2O)Si^{\bullet}$ moieties. They show considerable thermal stability, since they decrease their weight upon heating to 700 °C by only 10% and they do not change their whitish appearance, which is compatible with the absence of carbonization.

DOI: 10.1002/aoc

The XP and FTIR spectra and the EDX-SEM analyses are compatible with polyoxoazocarbosilane structure that undergoes thermally induced re-organization into silicon oxycarbonitride, which can be described as a network of interconnected Si, C, O and N atoms.

Acknowledgements

The authors thank Dr O. Šolcová for physical absorption measurements. The work was supported by the Ministry of Education, Youth and Sports of the Czech Republic (grant ME 684).

REFERENCES

1. Mantz RA, Jones PF, Chaffee KP, Lichtenhan JD, Gilman JW, Ismail IMK, Burmeister MJ. *Chem. Mater.* 1996; **8**: 1250.
2. Soraru GD, Liu Q, Interrante LV, Apple T. *Chem. Mater.* 1998; **10**: 4047.
3. Wilson AM, Zhank G, Eguchi K, Xing W, Yates B, Dahn JR. *Chem. Mater.* 1997; **9**: 1601.
4. Birot M, Pillot J-P, Dunoguès J. *Chem. Rev.* 1995; **95**: 1443.
5. Peuckert M, Vaahs T, Brück M. *Adv. Mater.* 1990; **2**: 398.
6. Soum A. *Silicon-containing Polymers*, Chapter 11. Kluwer Academic: Dodrecht, 2000.
7. Riedel R, Passing G, Schönefelder H, Brook RJ. *Nature* 1992; **355**: 714.
8. Cauchetier M, Croix O, Herlin N, Luce M. *J. Am. Ceram. Soc.* 1994; **77**: 993.
9. Herlin N, Luce M, Musset E, Cauchetier M. *J. Eur. Ceram. Soc.* 1994; **13**: 285.
10. Fusil S, Armand X, Herlin N, Cauchetier M. *Key Engng Mater.* 1997; **132–136**(Pt 1, Euro Ceramics V): 141.
11. El Kortobi Y, D'Espinose de la Caillerie J-B, Legrand A-P, Armand X, Herlin N. *Chem. Mater.* 1997; **9**: 632.
12. Corriu RJP. *Angew. Chem. Int. Edn* 2000; **39**: 1376.
13. Davazoglou D. *Thin Solid Films* 2003; **437**: 266.
14. Scopel WL, Fantini MCA, Alayo MI, Pereyra I. *Thin Solid Films* 2002; **413**: 59.
15. Alayo MI, Pereyra I, Scopel WL, Fantini MCA. *Thin Solid Films* 2002; **402**: 154.
16. del Prado A, San Andrés E, Mártil I, González-Díaz G, Bravo D, López FJ, Bohne W, Röhrich J, Selle B, Martínez FL. *J. Appl. Phys.* 2003; **93**: 8930.
17. Bae YW, Gallois B, Wilkens BJ, Olsen JE. *J. Electrochem. Soc.* 1998; **145**: 1902.
18. González-Luna R, Rodrigo MT, Jiménez C, Martínez-Duart JM. *Thin Solid Films* 1998; **317**: 347.
19. Pola J, Urbanová M, Bastl Z, Šubrt J, Papagiannakopoulos P. *J. Mater. Chem.* 2000; **10**: 1415.
20. Pola J, Bastl Z, Urbanová M, Šubrt J, Beckers H. *Appl. Organometal. Chem.* 2000; **14**: 453.
21. Kupčík J, Bastl Z, Šubrt J, Pola J, Papadimitrou VC, Prosmitis AV, Papagiannakopoulos P. *J. Anal. Appl. Pyrol.* 2001; **57**: 109.
22. Pola J, Urbanová M, Bastl Z, Beckers H. *J. Mater. Chem.* 1999; **9**: 2429.
23. Urbanová M, Bastl Z, Šubrt J, Pola J. *J. Mater. Chem.* 2001; **11**: 1557.
24. Pola J, Galíková A, Galík A, Blechta V, Bastl Z, Šubrt J, Ouchi A. *Chem. Mater.* 2002; **14**: 144.
25. Jasinski JM, Becerra R, Walsh R. *Chem. Rev.* 1995; **95**: 1203.
26. Benson SW. *Thermochemical Kinetics*. Wiley: New York, 1976.
27. Pola J, Taylor R. *J. Organometal. Chem.* 1993; **446**: 131.
28. Pola J, Ouchi A, Vacek K, Galíková A, Blechta V, Boháček J. *Solid State Sci.* 2003; **5**: 1079.
29. Poindexter EH, Warren WL. *J. Electrochem. Soc.* 1995; **142**: 2508.
30. Inokuma AT, Kurata Y, Hasegawa S. *J. Electrochem. Soc.* 1995; **142**: 2346.
31. Bogomolova LD, Jachkin VA, Prushinsky SA, Stryahilev D, Sazonov A, Nathan A. *J. Non-cryst. Solids* 2002; **297**: 247.
32. Cros Y, Krautwurm J. *J. Non-cryst. Solids* 1995; **187**: 385.
33. Wagner CD, in Briggs D, Seah MP (eds). *Practical Surface Analysis, Auger and X-ray Photoelectron Spectroscopy*, Vol. 1. Wiley: Chichester, 1994; 595.
34. Alexander MR, Short RD, Jones R, Stollenwerk M, Zabold J, Michaeli W. *J. Mater. Sci.* 1996; **31**: 1879.
35. Ingo GM, Zachetti N. *High. Temp. Sci.* 1990; **28**: 137.
36. Finster J, Klinkenberg E-D, Heeg J. *Vacuum* 1990; **41**: 1586.
37. *Infrared Structural Correlation Tables and Data Cards*, Miller RGJ, Willis HA (eds). Heyden & Son: London 1969.
38. Kriegsmann H. *Zeit. Electrochem.* 1957; **61**: 1088.
39. Nakanishi K. *Infrared Absorption Spectroscopy*. Holden-Day: San Francisco, CA, 1962.
40. Hurwitz FI, Meador MAB. *J. Sol-Gel Sci. Technol.* 1999; **14**: 75.
41. Wang F, Gill WN, Kirk CA, Apple T. *J. Non.-Cryst. Solids* 2000; **275**: 210.
42. Brus J, Kolář F, Machovič V, Svítilová J. *J. Non-Cryst. Solids* 2001; **289**: 62.